Visualizing Mie Resonances in Low-Index Dielectric Nanoparticles

Jing Zhou,[1,2] Ashwin Panday,[3] Yuntao Xu,[1] Xi Chen,[4] Long Chen,[4] Chengang Ji,[1] and L. Jay Guo[1,3,4,*]
[1]Department of Electrical Engineering and Computer Science, The University of Michigan, Ann Arbor, Michigan 48109, USA
[2]State Key Laboratory of Infrared Physics, Shanghai Institute of Technical Physics, Chinese Academy of Sciences, 500 Yutian Road, Shanghai 200083, China
[3]Macromolecular Science and Engineering, The University of Michigan, Ann Arbor, Michigan 48109, USA
[4]Applied Physics, The University of Michigan, Ann Arbor, Michigan 48109, USA

(Received 15 October 2017; published 18 June 2018)

Resonant light scattering by metallic and high-index dielectric nanoparticles has received enormous attention and found many great applications. However, low-index dielectric nanoparticles typically do not show resonant scattering behaviors due to poor light confinement caused by small index contrast. This Letter describes a simple and effective approach to drastically enhance the resonance effect of the low-index particles by partial metal dressing. Mie resonances of low-index nanoparticles can now be easily visualized by scattered light. This scattering peak depends on sphere size and has a reasonable linewidth. A size difference as small as 8 nm was resolved by a peak shift or even by color change. The scattering peak is attributed to the enhanced TE_{11} Mie resonance of the low-index nanospheres. The metal dress not only provides a high-reflection boundary, but also functions as an antenna to couple the confined light power to the far field, leading to scattering maxima in the spectra. Additionally, the enhanced TE_{11} Mie resonance in low-index nanoparticles features a considerable magnetic response due to the strong circulating displacement currents induced by the intensified E field despite of a low permittivity (hence low index) of the particles. The enhanced Mie resonances could be used to sense minute changes in size or refractive index of low-index nanoparticles and benefit a wide range of applications.

DOI: 10.1103/PhysRevLett.120.253902

Light scattering by small particles is a fundamental topic in electromagnetics and has attracted a lot of attention throughout modern history [1]. Among all the phenomena, resonant scattering is the most outstanding behavior because it can be easily detected by spectroscopy and features a strong local field, enabling various applications of nanoparticles [2–8]. Metallic nanoparticles with localized surface plasmon resonances have been extensively studied and practically utilized in surface enhanced spectroscopy and metamaterials [9–11]. Recently, high-index dielectric nanoparticles with strong Mie resonances drew considerable interest. Efficient field localization and negligible material absorption facilitate prominent Mie resonances, leading to an optical magnetic response and scattering manipulation [7,8,12–16]. For low-index dielectric nanoparticles, the Mie resonances are weak and broad due to poor light confinement caused by low reflection at particle boundaries, so that they are typically not visible in light scattering spectra. However, low-index dielectric nanoparticles, such as SiO_2 and polystyrene nanoparticles, have more applications than their high-index or even metallic counterparts. If pronounced Mie resonances can be realized, many potential applications can be envisioned. In this work, we introduce a metal dressing approach to enhance Mie resonances of low-index nanoparticles so that they can be easily visualized by scattered light. The metal dress improves the light confinement ability of the low-index nanoparticles by enhancing boundary reflection. In addition, the open configuration of the metal dress turns dark modes bright. We experimentally and theoretically investigated the metal-dressed SiO_2 nanospheres. While strong plasmonic resonance associated with the crescent shape structures [17,18] occur in sub-100 nm size particles, they become very weak in the NIR range for large particles. In this work, we found a significantly enhanced TE_{11} Mie mode in the visible range. Low order Mie resonances scale almost linearly with the particle size, allowing us to distinguish an 8 nm size difference. At this resonance, the strong circulating displacement currents induced by the intensified E field rather than high permittivity could result in considerable magnetic response. The enhanced Mie resonances could be used to sense minute changes in size or refractive index and thus benefit a lot of applications utilizing the low-index nanoparticles.

The metal-dressed SiO_2 nanospheres were created by a two-step metal deposition process by electron beam evaporation. First, a thin metal film was deposited on a transparent glass substrate. Then, a dilute solution of nanospheres was spin-casted on the metal film to create well-separated particle distribution. Finally, another thin metal film was deposited on top of the particle and on the first metal layer. With this process, each of the SiO_2

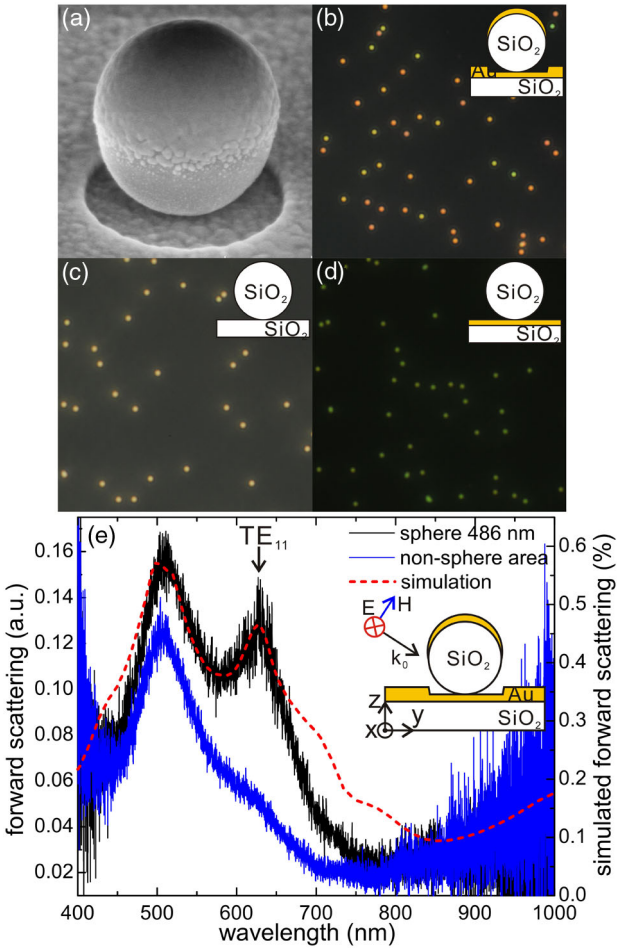

FIG. 1. (a) SEM image of a metal-dressed SiO_2 nanosphere. (b)–(d) Microscopic dark field transmission views of metal-dressed SiO_2 nanospheres, SiO_2 nanospheres on a fused silica substrate, and SiO_2 nanospheres on a 30 nm Au film over a fused silica substrate. (e) Measured forward scattering spectrum of a 486 nm nanosphere (black) together with simulation (red), and that at a blank area without nanospheres (blue). The simulated spectrum is normalized to the incident power. The incident E field is along the x axis.

nanospheres is partially covered by a metal cap and located in a shallow well in the metal film [Fig. 1(a)]. In our case, the substrate is fused silica and the deposited metal films are both Au, each with 30 nm thickness. According to SEM inspection, the sizes of the SiO_2 nanospheres range from 400 to 500 nm. In the microscopic dark field transmission view, the metal-dressed nanospheres exhibit different colors [Fig. 1(b)]. The NA of the dark field condenser is 0.80–0.95 and that of the objective is 0.75. In comparison, bare SiO_2 nanospheres could be identified [Fig. 1(c)], but shows no distinct color difference despite slightly different sizes because of their flat scattering spectra. At the middle stage of the two-step metal deposition process, where bare SiO_2 nanospheres are located on a thin Au film, there is also no color difference over individual nanospheres [Fig. 1(d)]. The greenish color comes from transmission through Au film, which allows a higher transmission of green light.

With a multimode fiber (core diameter ~200 nm), the dark field transmission of a single nanosphere could be selectively collected and analyzed by a spectrometer. Since the background transmission is significantly suppressed, the local property of any single metal-dressed nanosphere could be revealed by the spectrum. For example, the dark field transmission at a nanopshere with a diameter around 486 nm (size determined by SEM) is plotted in Fig. 1(e) (black curve). The peak around 510 nm is due to the interband transition in Au. This can be confirmed by analyzing the stray light through a blank area without any nanospheres but only the 60 nm Au film; the peak around 510 nm in the spectrum [blue curve in Fig. 1(e)] is attributed to the material property of Au film only. The peak around 630 nm is a resonance of the metal-dressed SiO_2 nanosphere and responsible for the distinctive colors. Simulations by finite element method were also performed for comparison. The forward scattering was simulated by integrating the transmitted power over a solid angle corresponding to the NA of the objective lens. The simulated spectrum [dashed red curve in Fig. 1(e)] agrees with the measurement (black curve) in terms of peak positions and profiles. The simulations were performed in three dimensions and the geometry followed the real sample. An oblique incidence with an angle 57° was used to mimic the dark field illumination.

Five nanospheres with size difference from 20 nm down to single digit nm are selected for spectral characterization [Fig. 2(a)]. The diameter of each nanosphere is obtained through SEM inspection of the same particle at a high magnification. In order to reduce the influence of the stray-light transmission peak from the thin Au film itself, the spectrum measured at a blank area is subtracted as a background from that measured at each nanosphere [Fig. 2(b)]. For example, the curve for nanosphere No. 5 is obtained by subtracting the blue curve from the black curve in Fig. 1(e), thus revealing the main peak associated with the resonance of the metal-dressed SiO_2 nanosphere. With the sphere size increasing from 421 to 486 nm, this peak is redshifted accordingly as confirmed by simulations (red dashed curves). It is worth noting that a size difference as small as 8 nm between nanosphere No. 1 and 2 could be clearly identified by the peak shift in spectrum, while they appear the same without the metal dressing. Since the Mie resonance is within the visible range, the peak shift due to size variation could also be distinguished by the color difference. As this resonance is redshifted with the increasing sphere size, the color of the nanospheres in the dark field transmission view varies from green to orange [Fig. 2(c)]. By calibrating colors with spectra, the sizes of the nanospheres could be read out directly through their colors with some accuracy [19]. In comparison, the SEM

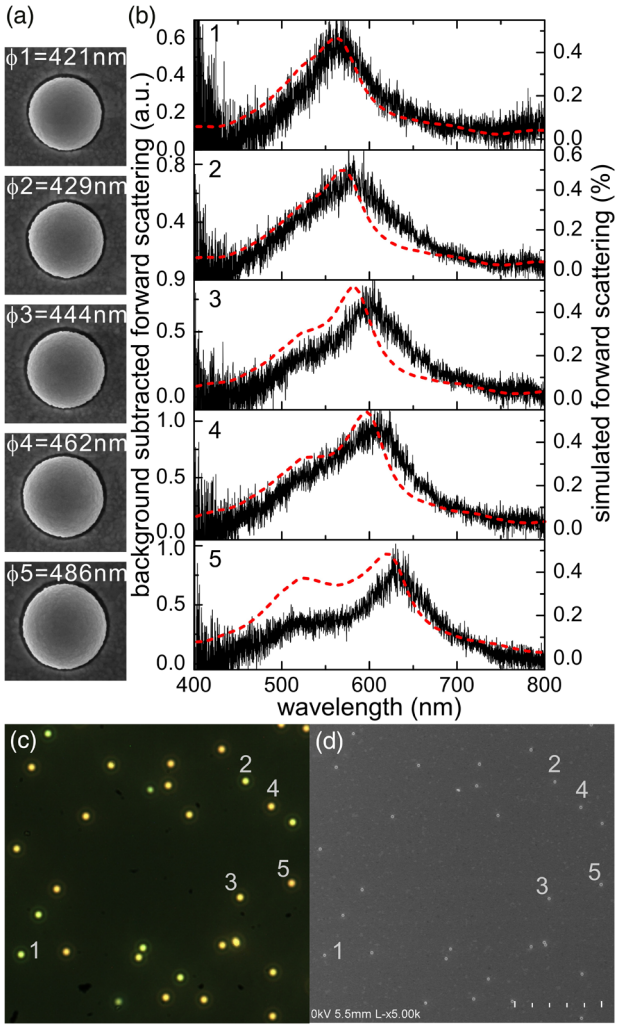

FIG. 2. (a) SEM images of five selected metal-dressed SiO_2 nanospheres with different sizes. (b) Background subtracted forward scattering spectra (black lines) of the five nanospheres and the corresponding simulations (dashed red lines). (c) Photopicture in the dark field transmission view for nanospheres including the five selected ones with size dependent colors. (d) SEM image of the same nanospheres in (c) with the same scope and the same magnification.

image [Fig. 2(d)] with the same field of view and the same magnification of the optical microscope image [Fig. 2(c)] fails to tell the size difference; only enlarging individual particles can tell its exact size. In addition, the enhanced Mie resonance is robust against small variations in the metal dressing. A 5 nm deviation in the thickness of each metal deposition step does not affect the resonant frequency [19].

The pronounced peak in the forward scattering spectra is revealed as an enhanced Mie resonance by comparing the metal-dressed SiO_2 nanospheres with complete-metal-shell ones. Figure 3(a) presents the scattering efficiency Q_{sc} of a complete-Au-shell SiO_2 nanosphere in air as a function of wavelength and core size based on Mie theory [1,24]. The shell thickness remains 30 nm. $Q_{sc} = [2/(k_0 r)^2] \sum_{n=1}^{\infty}(2n+1)(|a_n|^2 + |b_n|^2)$, where k_0 is free space wave vector, r is the core radius, a_n and b_n are coefficients of the scattered field decomposed in the basis of vector spherical harmonics [1,24]. Because of the tight light confinement provided by the metal shell, the Mie resonances of the SiO_2 nanosphere are significantly enhanced but become less radiant at the same time. Through interaction, the Mie resonances show up as Fano dips [cutting lines in Fig. 3(a)] in the background of the metal sphere scattering [25,26], leading to resonant scattering suppression. Figure 3(b) shows Q_{sc} at the core size of 550 nm and the decomposed contributions from the first three fundamental Mie modes: $Q_{a1} = 6|a_1|^2/(k_0 r)^2$, $Q_{b1} = 6|b_1|^2/(k_0 r)^2$, and $Q_{a2} = 10|a_2|^2/(k_0 r)^2$. a_1, b_1, and a_2 correspond to the TM_{11}, TE_{11}, and TM_{12} mode, respectively. TM (TE) stands for transverse magnetic (electric) modes with no radial magnetic (electric) field. The subscripts denote different orders. For a better comparison with our experiment, the complete-Au-shell nanosphere is located on a Au film and illuminated under the dark field scheme [Fig. 3(c) inset]. The Au film has a 30 nm indentation below the nanosphere and is 60 nm thick elsewhere. The shell merges with the Au plane at the bottom. As shown in Fig. 3(c), the Mie resonances are observed in the simulated forward scattering spectrum at the same wavelengths as those in Figs. 3(a) and 3(b). In this case, the three resonances are still less radiant and thus show Fano shapes in the background of the transmission through the Au film. The light field distribution at the TE_{11} resonance [Fig. 3(d)] reveals the mode pattern as an inclining magnetic dipole (MD) with electric field vortex circulating around it, as diagrammatically sketched by the inset of Fig. 3(c).

Figure 3(e) presents the simulated forward scattering spectrum of a metal-dressed SiO_2 nanosphere with a diameter around 486 nm. This spectrum is the same as the dashed red line in Fig. 1(e) but extended to longer wavelengths. Figure 3(f) presents the field distribution at the resonance (~630 nm). A direct comparison between Figs. 3(d) and 3(f) reveals that the pronounced peak we observed in experiment corresponds to the enhanced TE_{11} Mie resonance of the SiO_2 nanosphere. In another model, the enhanced TE_{11} Mie mode could be considered as a Fabry-Perot (FP) resonance of a waveguide mode propagating at a tilted angle [Fig. 3(f)]. Compared to the mode pattern of the metal-sandwiched cylindrical waveguide, the light field inside the metal-dressed sphere could be regarded as a standing wave of the waveguide mode due to multiple reflections [19]. The waveguide mode FP resonance in our configuration is a localized mode confined in the metal-dressed nanoparticle, and therefore insensitive to the incident angle. Although a complete metal shell provides a better light confinement than the metal dress as revealed by the higher field concentration inside the SiO_2

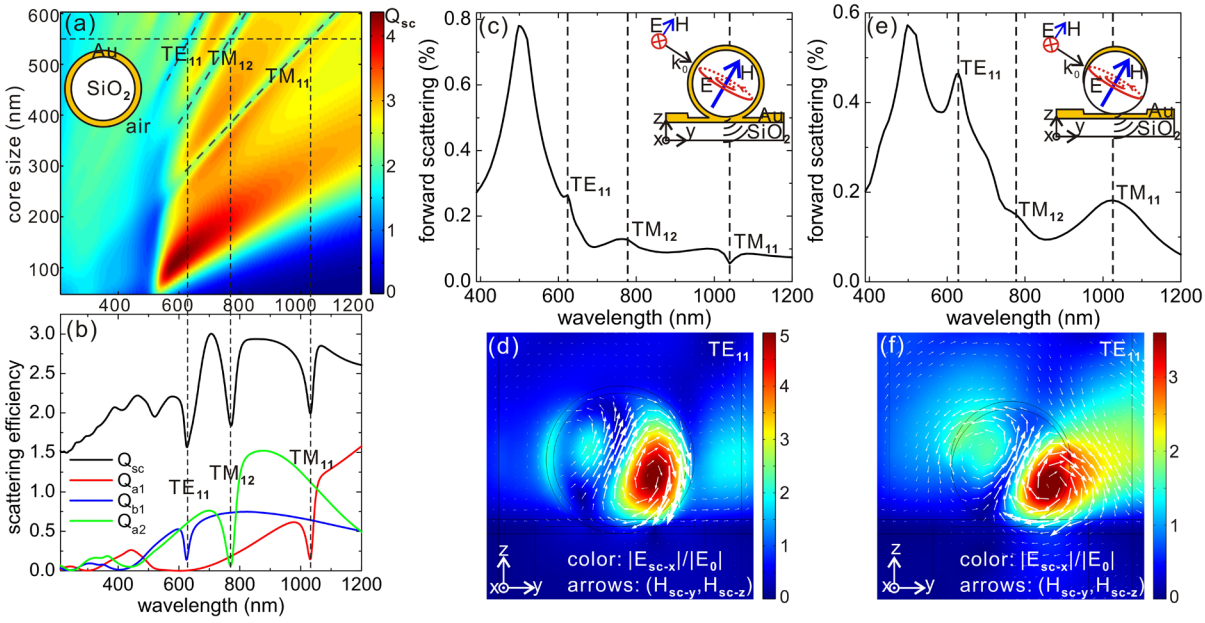

FIG. 3. (a) Scattering efficiency (Q_{sc}) spectrum at different core sizes of the complete-shell nanosphere (shell thickness 30 nm) in air. (b) Q_{sc} spectrum at the core size of 550 nm [indicated by the horizontal dashed line in (a)] and the decomposed contributions from the first three fundamental Mie modes (TM_{11}, TE_{11}, and TM_{12}). (c) Forward scattering spectrum of the complete-shell nanosphere (core size 550 nm) located on a Au film under dark field illumination. (d) Distributions of scattered electric field x component $|E_{sc-x}|$ and scattered in-plane magnetic field vector (H_{sc-y}, H_{sc-z}) at the TE_{11} resonance on the y-z plane at $x = 0$. (e) and (f) Forward scattering spectrum and field distribution of the metal-dressed nanosphere (486 nm) at the TE_{11} resonance.

nanosphere [comparison between Figs. 3(d) and 3(f)], the metal dress is much more favorable to fabrication. Core-shell structures below 100 nm could be created by chemical synthesis [27]. However, making larger shells (several hundred nm to 1 μm) is much tougher than making a metal dress by a two-step deposition. Further, the Mie resonances in the metal-dressed nanosphere appear as peaks in scattering spectra [Fig. 1(e) and Fig. 3(e)], while the Mie resonances in the complete-shell nanosphere appear as Fano dips [Figs. 3(a)–3(c)]. The metal dress not only enhances the Mie resonances by providing high reflecting boundaries but also couples the Mie mode into the far field by serving as an antenna.

The enhanced TE_{11} Mie resonance is associated with a MD resonance since the field distribution [Fig. 3(f)] shows circulating displacement currents and an intensified magnetic field at the center. Actually, the ideal TE_{11} Mie resonance of a nanosphere could just be regarded as a MD resonance [1]. The magnetic response of high-index dielectric nanoparticles is mainly due to that and has attracted much attention [7,8,12]. Since the circulating displacement current density [$J_D = (-i\omega)\varepsilon_0\varepsilon_r E$] as well as the induced MD increases with permittivity, prominent magnetic responses are observed. From another point of view, one need not rely solely on the high refractive index to produce strong magnetic resonances if a strong E field can be obtained [12]. Typically, an intensified E field can be obtained in an optical cavity with high Q-factor modes. Since low-index particles provide very weak light confinement and therefore low-Q Mie modes, they typically are not suited for inducing magnetic response. However, with help of the metal dressing, the Mie modes of low-index nanoparticles are greatly enhanced. At the TE_{11} mode [Fig. 3(f)], the strong circulating electric field leads to strong circulating displacement currents and thus a strong MD. This result implies that considerable magnetic response could also be induced in low-index nanoparticles by a simple metal dressing process. Nevertheless, due to the induced currents in the metal dress, the optical response at the TE_{11} Mie resonance is not a pure MD response. Other components could be identified by a multipole decomposition calculation based on the simulated light field distributions [19]. In the view of method of images, the tilted MD on a Au film could be considered as the MD with its image and the appearance of high order multipoles is reasonable [19].

The enhanced Mie resonance is distinguished from plasmon modes. The Mie mode is concentrated within the SiO_2 nanosphere as an optical cavity while plasmon modes are typically at metal and dielectric interfaces [19]. Moreover, the Mie mode is also different from split ringlike resonances, associated with highly concentrated field within the split gaps [28], although the metal dress shares some similarities with a split shell. The metal dressing process has also been applied to semiconductor nanorods with high refractive index for plasmonic cloaking [29,30] and nanoscale color filtering [31]. For deep-subwavelength sizes, when the induced electric dipole moment in the core and that in the shell are equal in magnitude but opposite in

sign, scattering cancellation is realized. For spheres with larger sizes in our case, phase retardation plays a role and Mie modes become the key factor of scattering properties.

The enhanced Mie resonances as local modes could be utilized for sensing the individual low-index nanospheres. Low-index nanoparticles such as SiO_2 and polystyrene nanospheres have a wide range of important applications [32–38]. Sensing the local properties of individual nanoparticles, such as size and refractive index, in a proper manner would greatly benefit all those applications. The enhanced Mie resonances as peaks in scattering spectra could work for sensing. Since the resonance occurs in the visible range, the minute size difference could also be sensed by color difference. After mapping the particle size with color, we could obtain the sizes of all the nanospheres in one micrograph by analyzing their colors. Compared to SEM inspection and dynamic light scattering, this colorimetric approach could lead to a new particle sizing method with both efficiency and accuracy [19]. When particle size is fixed, a minute change in the refractive index of the particle could be sensed by a shift of the enhanced Mie resonance [19].

In summary, the metal dress created by a two-step deposition process prominently enhances the Mie resonances of low-index nanoparticles. The metal dress improves the light confinement ability of low-index nanoparticles by enhancing boundary reflection and thus enhances the Mie resonances. Beyond a high reflection cavity, the metal dress also functions as a broadband antenna to couple the concentrated light power to the far field. The resonance occurring in the visible range leads to size dependent colors. At the enhanced TE_{11} Mie resonance, the intensified E field instead of high permittivity induces strong circulating displacement currents and thus considerable magnetic response. The enhanced Mie resonances could be used to sense minute changes in size or refractive index of low-index nanoparticles and benefit many applications.

The authors appreciate the discussion with You-chia Chang about the spectrum measurement of a single nanoparticle. This work is supported in part by the NSF Grant No. DMR 1120923; J. Z. acknowledges the support by the National Key Research and Development Program of China Grant No. 2017YFA0205801, the Hundred Talent Program of the Chinese Academy of Sciences, the National Natural Science Foundation of China Grant No. 61605230 and No. U1737111, and the Shanghai Pujiang Program 16PJ1410400.

*guo@umich.edu

[1] C. F. Bohren and D. R. Huffman, *Absorption and Scattering of Light by Small Particles* (Wiley, New York 1983).

[2] K. L. Kelly, E. Coronado, L. L. Zhao, and G. C. Schatz, The optical properties of metal nanoparticles: The influence of size, shape, and dielectric environment, J. Phys. Chem. B **107**, 668 (2003).

[3] K.-S. Lee and M. A. El-Sayed, Gold and silver nanoparticles in sensing and imaging: sensitivity of plasmon response to size, shape, and metal composition, J. Phys. Chem. B **110**, 19220 (2006).

[4] J. N. Anker, W. P. Hall, O. Lyandres, N. C. Shah, J. Zhao, and R. P. Van Duyne, Biosensing with plasmonic nanosensors, Nat. Mater. **7**, 442 (2008).

[5] A. I. Kuznetsov, A. E. Miroshnichenko, M. L. Brongersma, Y. S. Kivshar, and B. Luk'yanchuk, Optically resonant dielectric nanostructures, Science **354**, aag2472 (2016).

[6] J. C. Ginn and I. Brener, Realizing Optical Magnetism from Dielectric Metamaterials, Phys. Rev. Lett. **108**, 097402 (2012).

[7] L. Shi, T. U. Tuzer, R. Fenollosa, and F. Meseguer, A new dielectric metamaterial building block with a strong magnetic response in the sub-1.5-micrometer region: Silicon colloid nanocavities, Adv. Mater. **24**, 5934 (2012).

[8] A. B. Evlyukhin, S. M. Novikov, U. Zywietz, R. L. Eriksen, C. Reinhardt, S. I. Bozhevolnyi, and B. N. Chichkov, Demonstration of magnetic dipole resonances of dielectric nanospheres in the visible region, Nano Lett. **12**, 3749 (2012).

[9] S. Nie and S. R. Emory, Probing single molecules and single nanoparticles by surface-enhanced raman scattering, Science **275**, 1102 (1997).

[10] S. Lal, S. Link, and N. J. Halas, Nano-optics from sensing to waveguiding, Nat. Photonics **1**, 641 (2007).

[11] J. A. Fan, C. Wu, K. Bao, J. Bao, R. Bardhan, N. J. Halas, V. N. Manoharan, P. Nordlander, G. Shvets, and F. Capasso, Self-assembled plasmonic nanoparticle clusters, Science **328**, 1135 (2010).

[12] B.-I. Popa and S. A. Cummer, Compact Dielectric Particles as a Building Block for Low-Loss Magnetic Metamaterials, Phys. Rev. Lett. **100**, 207401 (2008).

[13] Y. H. Fu, A. I. Kuznetsov, A. E. Miroshnichenko, Y. F. Yu, and B. Luk'yanchuk, Directional visible light scattering by silicon nanoparticles, Nat. Commun. **4**, 1527 (2013).

[14] S. Zhang, R. Jiang, Y.-M. Xie, Q. Ruan, B. Yang, J. Wang, and H.-Q. Lin, Colloidal moderate-refractive-index Cu_2O nanospheres as visible-region nanoantennas with electromagnetic resonance and directional light-scattering properties, Adv. Mater. **27**, 7432 (2015).

[15] S. Person, M. Jain, Z. Lapin, J. J. Sáenz, G. Wicks, and L. Novotny, Demonstration of zero optical backscattering from single nanoparticles, Nano Lett. **13**, 1806 (2013).

[16] A. E. Miroshnichenko, A. B. Evlyukhin, Y. F. Yu, R. M. Bakker, A. Chipouline, A. I. Kuznetsov, B. Luk'yanchuk, B. N. Chichkov, and Y. S. Kivshar, Nonradiating anapole modes in dielectric nanoparticles, Nat. Commun. **6**, 8069 (2015).

[17] M. Cortie and M. Ford, A plasmon-induced current loop in gold semi-shells, Nanotechnology **18**, 235704 (2007).

[18] J. B. Lassiter, M. W. Knight, N. A. Mirin, and N. J. Halas, Reshaping the plasmonic properties of an individual nanoparticle, Nano Lett. **9**, 4326 (2009).

[19] See Supplemental Material at http://link.aps.org/supplemental/10.1103/PhysRevLett.120.253902 for the influence of the metal thickness on the enhanced resonance, optical responses of uncoated SiO_2 nanospheres and the shallow nano wells, further comparison between the complete-shell SiO_2 nanosphere and the metal-dressed

SiO_2 nanosphere, analysis based on the method of images, modeling by waveguide mode FP resonances, angle dependence of the enhanced resonance; plasmon modes of the metal dress, particle sizing by the colorimetric method, and index sensing based on the enhanced resonance, which includes Refs. [20–23].

[20] I. Staude, A. E. Miroshnichenko, M. Decker, N. T. Fofang, S. Liu, E. Gonzales, J. Dominguez, T. S. Luk, D. N. Neshev, I. Brener, and Y. Kivshar, Tailoring directional scattering through magnetic and electric resonances in subwavelength silicon nanodisks, ACS Nano **7**, 7824 (2013).

[21] J. van de Groep and A. Polman, Designing dielectric resonators on substrates: Combining magnetic and electric resonances, Opt. Express **21**, 26285 (2013).

[22] M. Decker, I. Staude, M. Falkner, J. Dominguez, D. N. Neshev, I. Brener, T. Pertsch, and Y. S. Kivshar, High-efficiency dielectric huygens' surfaces, Adv. Opt. Mater. **3**, 813 (2015).

[23] Y. Yamaguchi, Y. Yamada, and J. Ishii, Supercontinuum-source-based facility for absolute calibration of radiation thermometers, Int. J. Thermophys. **36**, 1825 (2015).

[24] C. Mätzler, MATLAB Functions for Mie Scattering and Absorption, Institut für Angewandte Physik, Research Report No. 2002-08, Bern, Switzerland, 2002.

[25] W. Chaabani, A. Chehaidar, and J. Plain, Comparative theoretical study of the optical properties of silicon/gold, silica/gold core/shell and gold spherical nanoparticles, Plasmonics **11**, 1525 (2016).

[26] J. S. Parramon and D. Jelovina, Boosting Fano resonances in single layered, Nanoscale **6**, 13555 (2014).

[27] S. J. Oldenburg, R. D. Averitt, S. L. Westcott, and N. J. Halas, Nanoengineering of optical resonances, Chem. Phys. Lett. **288**, 243 (1998).

[28] A. I. Kuznetsov, A. E. Miroshnichenko, Y. H. Fu, V. Viswanathan, M. Rahmani, V. Valuckas, Z. Y. Pan, Y. Kivshar, D. S. Pickard, and B. Luk'yanchuk, Split-ball resonator as a three-dimensional analogue of planar split-rings, Nat. Commun. **5**, 3104 (2014).

[29] P. Fan, U. K. Chettiar, L. Cao, F. Afshinmanesh, N. Engheta, and M. L. Brongersma, An invisible metal–semiconductor photodetector, Nat Photon. **6**, 380 (2012).

[30] A. Alù and N. Engheta, Achieving transparency with plasmonic and metamaterial coatings, Phys. Rev. E **72**, 016623 (2005).

[31] J. K. Hyun, T. Kang, H. Baek, D.-s. Kim, and G.-c. Yi, Nanoscale single-element color filters, Nano Lett. **15**, 5938 (2015).

[32] C. L. Haynes and R. P. Van Duyne, Nanosphere lithography: A versatile nanofabrication tool for studies of size-dependent nanoparticle optics, J. Phys. Chem. B **105**, 5599 (2001).

[33] I. I. Slowing, B. G. Trewyn, S. Giri, and V. S.-Y. Lin, Mesoporous silica nanoparticles for drug delivery and biosensing applications, Adv. Funct. Mater. **17**, 1225 (2007).

[34] M. Liong, J. Lu, M. Kovochich, T. Xia, S. G. Ruehm, A. E. Nel, F. Tamanoi, and J. I. Zink, Multifunctional inorganic nanoparticles for imaging, targeting, and drug delivery, ACS Nano **2**, 889 (2008).

[35] M. De, P. S. Ghosh, and V. M. Rotello, Applications of nanoparticles in biology, Adv. Mater. **20**, 4225 (2008).

[36] J. Kim, H. S. Kim, N. Lee, T. Kim, H. Kim, T. Yu, I. C. Song, W. K. Moon, and T. Hyeon, Multifunctional uniform nanoparticles composed of a magnetite nanocrystal core and a mesoporous silica shell for magnetic resonance and fluorescence imaging and for drug delivery, Angew. Chem., Int. Ed. **47**, 8438 (2008).

[37] J. Bravo, L. Zhai, Z. Wu, R. E. Cohen, and M. F. Rubner, Transparent superhydrophobic films based on silica nanoparticles, Langmuir **23**, 7293 (2007).

[38] M. Manca, A. Cannavale, L. De Marco, A. S. Arico, R. Cingolani, and G. Gigli, Durable superhydrophobic and antireflective surfaces by trimethylsilanized silica nanoparticles-based sol-gel processing, Langmuir **25**, 6357 (2009).